



**UNIVERSITY OF LEEDS**

This is a repository copy of *Flame extinctions: Critical stretch rates and sizes*.

White Rose Research Online URL for this paper:

<http://eprints.whiterose.ac.uk/153798/>

Version: Accepted Version

---

**Article:**

Bradley, D, Shehata, M, Lawes, M et al. (1 more author) (2020) Flame extinctions: Critical stretch rates and sizes. *Combustion and Flame*, 212. pp. 459-468. ISSN 0010-2180

<https://doi.org/10.1016/j.combustflame.2019.11.013>

---

© 2019 Published by Elsevier Inc. on behalf of The Combustion Institute. This manuscript version is made available under the CC-BY-NC-ND 4.0 license  
<http://creativecommons.org/licenses/by-nc-nd/4.0/>.

**Reuse**

This article is distributed under the terms of the Creative Commons Attribution-NonCommercial-NoDerivs (CC BY-NC-ND) licence. This licence only allows you to download this work and share it with others as long as you credit the authors, but you can't change the article in any way or use it commercially. More information and the full terms of the licence here: <https://creativecommons.org/licenses/>

**Takedown**

If you consider content in White Rose Research Online to be in breach of UK law, please notify us by emailing [eprints@whiterose.ac.uk](mailto:eprints@whiterose.ac.uk) including the URL of the record and the reason for the withdrawal request.



[eprints@whiterose.ac.uk](mailto:eprints@whiterose.ac.uk)  
<https://eprints.whiterose.ac.uk/>

# Flame Extinctions: Critical Stretch Rates and Sizes

D. Bradley\*, M. Shehata, M. Lawes, Pervez Ahmed

School of Mechanical Engineering, University of Leeds, Leeds LS2 9JT, United Kingdom

\*Corresponding author

\*E-mail address: [d.bradley@leeds.ac.uk](mailto:d.bradley@leeds.ac.uk)

## Abstract

The paper reports how experimental data from a fan-stirred explosion vessel have extended the boundary of the previously defined regime, within which stable premixed turbulent combustion occurs. It also defines the properties of the bordering regime of turbulent flame quenching.

The combustion regime is defined by the normalised turbulent burning velocity,  $U$ , the Karlovitz stretch factor,  $K$ , and strain rate Markstein number,  $Ma_{sr}$ . The data cover hydrogen, methane, and higher hydrocarbons, at different equivalence ratios and pressures.

In contrast, the flame quench regime is defined by the mean diameters of flame kernels at quench, normalised by their laminar flame thickness,  $d_k/\delta_k$ . These values must be exceeded to initiate a propagating flame. Values of  $d_k/\delta_k$  increase with both  $K$  and  $Ma_{sr}$ .

It is also shown, that the flame extinction at blow-off of non-premixed jet flames, is closely related to the observed single kernel quenching of premixed flames. With jet flames, the flow number,  $U^*$ , has similarities with  $K$ . The normalised jet burner diameters,  $D_b/\delta_k$ , change with  $U^*$ , in a similar fashion to the way  $d_k/\delta_k$  changes with  $K$  for premixed flames.

Finally, the way in which highly turbulent premixed flames can survive extinction by the entrainment of flame gases from a pilot flame is analysed.

## Key words

Flame quenching, 2D schlieren cine, 3D swinging laser sheet imaging, Jet flames, Quenching stretch rate, Critical quenching diameters.

## Nomenclature

$c_p$	Specific heat (J/kg.K)
$D$	Thermal diffusivity (m <sup>2</sup> /s), also pipe diameter (m)
$D_b$	Jet pipe diameter at blow-off, $D_k$
$d_k$	Maximum mean diameter of quenched flame kernel
$f$	Focal length (mm), mass fraction of burned gas
$K$	Karlovitz stretch factor, $0.25(u'/u_l)^2 R_l^{-0.5}$
$Ka$	Karlovitz number $\cong 15^{0.5} K$
$K_{ql}$	laminar flame extinction stretch factor, $(\alpha_q \delta_l / u_l)$ .
$k$	Thermal conductivity (W/m.K)
$\bar{k}_\eta$	Dimensionless wave number
$L$	Integral length scale
$Le$	Lewis number
$Ma_{sr}$	Markstein number for strain rate
$N_f$	Fan speed (rpm)
$P_i/P_a$	Pressure ratio of initial stagnation to atmospheric pressure
$p_b$	Probability of burning
$R_L$	Turbulent Reynolds number based on turbulent integral length scale
$R_\lambda$	Turbulent Reynolds number based on Taylor microscale, $u' \lambda / \nu$
$r$	Radius of the flame kernel
$s_{q+}$	Flame extinction positive stretch rate (s <sup>-1</sup> )
$s_{q-}$	Flame extinction negative stretch rate (s <sup>-1</sup> )
$\bar{S}(\bar{k}_\eta)$	Non-dimensional power spectral density
$T_u$	Mixing temperature (K)
$U$	Normalised turbulent burning velocity, $u_t/u'_k$
$U^*$	Flow number for flame blow-off in jet, $(u/u_{lm})(\delta_k/D)^{0.4}(P_i/P_a)$ .
$u$	Mean velocity in burner, also, fuel flow mean velocity at the pipe exit for subsonic flow. (m/s)
$u'$	rms velocity (m/s)
$u'_k$	Effective rms turbulent velocity (m/s)
$u_l$	Laminar burning velocity (m/s)
$u_{lm}$	Maximum laminar burning velocity of the fuel–air mixture (m/s)
$u_t$	Turbulent burning velocity (m/s)
$u_\eta$	Kolmogorov velocity (m/s)
Greek	
$\alpha$	Mass diffusivity of the deficient reactant (m <sup>2</sup> /s), also, stretch rate (s <sup>-1</sup> )
$\alpha_q$	Laminar extinction stretch rate (s <sup>-1</sup> )
$\delta_l$	Laminar flame thickness (m) , $\nu/u_l$
$\delta_k$	Preheat zone flame thickness = $(k/C_p)T^\circ/(\rho_u u_l)$
$\varphi$	Equivalence ratio
$\rho_b$	Burned gas density (kg/m <sup>3</sup> )
$\rho_u$	Unburned gas density (kg/m <sup>3</sup> )
$\lambda$	Taylor length scale (m)
$\eta$	Kolmogorov length scale (m)
$\nu$	kinematic viscosity (m <sup>2</sup> /s)

$\tau_c$	Chemical time scale (s), $(\delta_l/u_l)$
$\tau_\eta$	Kolmogorov time scale (s), $(\eta/u_\eta)$

#### Abbreviations

IL	Imaging laser
I <sub>g</sub> L	Ignition laser
RM	Rotating mirror
YAG	Yttrium Aluminum Garnet

## 1. Introduction

Flame quenching usually occurs as a result of compositional change, increasing aerodynamic strain rate, or heat loss, making the mixture less reactive. Extinction stretch rates,  $\alpha_q$ , have been measured under steady state conditions, but can be exceeded in short time transients, without ensuing extinctions [1]. Flame quenching has been studied under varied experimental conditions, in burners [2-5], test tubes [6], orifices [7, 8], and closed vessels [9-12].

The paper presents the results of an experimental study of explosion flames in a fan-stirred vessel of both Karlovitz stretch factor, and, additionally, mean kernel diameters at extinction, normalised by their laminar flame thickness.

Five major aspects are covered: *(i)* Use of a swinging laser sheet to study kernel shape and whether a mean quenching diameter is a valid parameter, *(ii)* Measurement and correlation of normalised kernel quenching diameters, *(iii)* Development of a unified approach to both premixed and non-premixed jet extinctions, *(iv)* Revision of previous boundary for turbulent flame extinctions, *(v)* Use of pilot flame entrainment by highly turbulent premixed flames to counter their extinction.

Extinction stretch rates have been employed rather more widely than kernel extinction sizes in flame quenching studies, in both measurements [3] and chemical kinetic computations have covered laminar extinction stretch rates, over wide ranges of stretch rates, fuels, equivalence ratios, and Lewis numbers [2] in symmetrical counter-flow, and twin- flame configurations.

Experimental extinction stretch rates [3] have been compared with chemically kinetic computed values [13, 14] and [15] for CH<sub>4</sub> and C<sub>3</sub>H<sub>8</sub>, with numerical results tending to over-predict measured values. It is convenient to generalise extinction in terms of a Karlovitz laminar flame extinction stretch factor,  $K_{ql}$ , equal to the stretch rate,  $\alpha_q$ , normalised by the chemical time, the laminar flame thickness divided by the laminar burning velocity.

Egolfopoulos and co-workers have studied extinctions in both premixed and diffusion counter-flow flames, both measuring [5, 16-21], and chemical kinetically modelling [14, 22, 23], values of  $\alpha_q$ . Experimentally [16], they found lean *i*-octane and *n*-heptane to be more readily quenched than lean alcohol flames. In [20] values of  $\alpha_q$  for *n*-butanol were measured experimentally and simulated numerically, using kinetic models [24, 25]. There was good agreement between the experimental values in [20] and the skeletal Westbrook mode in [24], despite an over-prediction in  $\alpha_q$  of up to 15% for rich *n*-butanol. This was unlike the skeletal Dagaut model [25], which over-predicted it by 40%. Extinction trends are similar for ethanol and *n*-butanol/ air mixtures [20]. Experimental studies of non-premixed flames [26] with single component hydrocarbons, surrogates, and jet fuels, found the higher carbon fuels to be less resistant to quench, as the non-premixed low carbon fuels are more diffusive. Similarly, a comparative study [27], showed H<sub>2</sub>/air mixtures [17] to be the most resistant to quench, in comparison with *i*-octane [16], CH<sub>4</sub> and C<sub>3</sub>H<sub>8</sub> [3], possibly due to the more diffusive molecules of H<sub>2</sub>.

Klimov [28] and Williams [29] have pioneered the study of turbulent flame quenching. They proposed a correlating parameter of the Kolmogorov scale strain rate multiplied by the laminar flame chemical time, comprised of the laminar flame thickness divided by the laminar burning velocity. This Klimov-Williams criterion for turbulent flame quenching suggested it occurred when the associated Karlovitz number exceeded unity. Kuznetsov [30] employed a similar chemical to eddy lifetime criterion, but with the latter given by  $L/u'$ , where,  $L$  is the turbulent integral length scale, and  $u'$  the rms turbulent velocity. Abdel-Gayed et al. [31] employed  $\lambda/u'$  for this parameter, with  $\lambda$  the Taylor scale. They demonstrated the nature of turbulent flame quenching through schlieren images of fragmenting and quenching flame kernels in a cylindrical explosion vessel with fan-generated turbulence, and showed a quenching regime dependence upon Lewis number. The complexities of practical flows can ensure that reaction ultimately occurs in a particular region through their vagaries.

Shy et al. [32] showed that the radiative heat losses to affect the turbulent burning velocities of rich diluted CH<sub>4</sub> flames, with increasing turbulence intensity, whilst Liu et al. [33] showed their effect on CO<sub>2</sub>-diluted and N<sub>2</sub>-diluted flames. The critical Karlovitz number for quenching of N<sub>2</sub>-diluted CH<sub>4</sub> flames with low radiative heat losses was found to be higher than CO<sub>2</sub>-diluted CH<sub>4</sub> flames with higher losses.

Meneveau and Poinso [34] evaluated the role of the stretch rate of flamelets using direct numerical simulations of vortex-flame interaction and a model of intermittent turbulence. The onset of flame quenching was expressed in plots of  $u'/u_l$  against  $L/\delta$ , with high values of  $u'/u_l$ , occurring for  $L/\delta \leq 10$  in [35]. They cautioned that quenching is a strong function of heat losses and that these are difficult to estimate in experiments. Both [31] and [35] show the Klimov-Williams criterion to overestimate the flame quenching. Upper and lower limits of quenching are shown in an extended Borghi diagram in [36]. The upper limit results from the direct numerical simulations, DNS, in [35], and the lower limit from the Klimov-Williams theory [37, 38]. These aspects can be seen in Fig.11.

A probability density function, pdf, of strain rates, derived from the DNS of Yeung et al. [39] enables pdfs of flame stretch rate to be generated [40]. With the lower and upper stretch bounds, these yield theoretical values of flame propagation probabilities.

In [41], with a strain rate based on the Taylor scale,  $\lambda$ , a Karlovitz stretch factor,  $K$ , is defined in terms of a chemical, to eddy lifetime ratios, with  $K = \frac{\delta_l/u_l}{\lambda/u'}$ , with the “eddy lifetime” the inverse of the strain rate. From this it can be shown, that, with an appropriate relationship between  $\lambda$  and  $L$  [41],

$$K = 0.25(u'/u_l)^2 R_l^{-0.5}. \quad (1)$$

In the early stages of spherical explosive flame propagation, the flame can be wrinkled only by length scales less than the flame kernel radius,  $r$ . An effective rms velocity at  $r$  is  $u'_k$ , less than  $u'$ . Evaluation of  $u'_k/u'$  is by integrating the non-dimensional power spectral density, over the relevant range of wavelengths, as described in [41].

The effective rms velocity,  $u'_k$  at any instant is defined by [41, 42]:

$$u'_k = u' \left[ \frac{\sqrt{15}}{R_\lambda} \int_{\bar{k}_{\eta 1}}^{\bar{k}_{\eta 2}} \bar{S}(\bar{k}_\eta) d\bar{k}_\eta \right]^{0.5}, \quad (2)$$

where  $\bar{S}(\bar{k}_\eta)$  is a non-dimensional power spectral density over a wide range of  $R_\lambda$ . The lower limit,  $\bar{k}_{\eta 1}$ , the flame diameter and the upper limit,  $\bar{k}_{\eta 2}$ , the Kolmogorov length scale [41]. This limit was also evaluated using the Gibson scale [42]. Power spectral densities and other turbulence characteristic of the vessel, at different fan speeds, measured by particle image velocimetry, are given in [43].

In [44, 45] turbulent burning velocities,  $u_t$ , are normalised by  $u'_k$ , to give  $U$ . The strain rate influences upon  $U$  are expressed by a combination of  $K$ , and the strain rate Markstein number,  $Ma_{sr}$ . Values of  $U$  are plotted against those of  $K$ , with values of  $Ma_{sr}$  also shown, as in the present Fig. 10.

Because of the importance of the smaller length scales in quenching, it might be thought advantageous to plot these values against a Karlovitz number,  $Ka$ , based on the smaller Kolmogorov eddy time scale,  $\tau_\eta = \eta/u_\eta$ . However, this anticipation holds no further advantage because it can be shown that  $Ka/K \approx 15^{0.5}$ .

Probabilities of flame propagation, as distinct from extinction, have been measured in the Leeds fan-stirred explosion vessel, with values of  $u'$  up to 7 m/s [11]. For different fuel/air mixtures at different  $\phi$ , and pressures up to 1.5 MPa, the measured probabilities of 80%,  $p_{0.8}$ , and 20%,  $p_{0.2}$ , for continuing flame propagation were expressed as a function of  $K$  and  $Ma_{sr}$  by [11]:

$$K(Ma_{sr} + 4)^{1.4} = 37.1 \quad \text{at} \quad -3 \leq Ma_{sr} \leq 11 \quad \text{for, } p_{0.2}, \text{ and} \quad (3)$$

$$K(Ma_{sr} + 4)^{1.8} = 34.4 \quad \text{at} \quad -3 \leq Ma_{sr} \leq 11 \quad \text{for } p_{0.8}. \quad (4)$$

Such probabilities were compared with theoretical flame propagation probabilities, derived by integrating the flame stretch rate probabilities between the appropriate limits [11]. Theoretical limitations arise from uncertainties in the positive and negative flame extinction stretch rates.

A demarcation boundary was plotted, within which there could be stable turbulent flames with  $U$  versus  $K$  relationships, including  $Ma_{sr}$ , based on measurements of explosions in the fan-stirred explosion vessel. The present paper revises this previous demarcation curve.

Just outside this regime of near quench is one in which an isolated flame kernel might briefly propagate to a maximum flame diameter, at which propagation ceases and the hot gases dissipate. A methodology was developed for measuring such limiting mean quenching kernel diameters in the fan-stirred vessel. Experimental data are presented for hydrocarbon and hydrogen mixtures at different pressures, temperatures, and rms turbulent velocities.

Measured quench diameters are normalised by the laminar flame thickness of the mixture, given by the expression of Götting et al. [46]. It identifies an inner layer, the thickness of which is defined by the location of a temperature  $T^0$ , below which there is no reaction. Calculated values of  $T^0$  are presented in [46]. The chemically inert preheat zone thickness is:

$$\delta_k = (k/Cp)|_{T^0}/(\rho_u u_l) \quad (5)$$

in which  $k$  and  $c_p$  are the thermal conductivity and specific heat at constant pressure at the inner layer temperature,  $T^0$ . The unburned gas density is  $\rho_u$ . Values of all the required physicochemical data were obtained from the Gaseq code [47].

Analyses of turbulent flame propagation and quench are extended to two further areas. The first concerns non-premixed jet flames sustained by the entrainment of air by the fuel jet. This can quench the flame at high jet velocities and small pipe diameters. The second concerns sustaining highly turbulent premixed flames by the entrainment of flame gases from a surrounding pilot flame to prevent turbulent flame extinction.

## 2. Experimental Methods

High speed photography, including swinging laser sheet imaging, revealed the details of flame quenching and enabled normalised quenched kernel diameters to be correlated with the Karlovitz stretch factor,  $K$ . Measurements were at constant pressure in a stainless steel, spherical explosion, fan-stirred vessel, MKII [48, 49], with an internal diameter of 380 mm. Three orthogonal pairs of quartz windows of 150 mm diameter and 100 mm thickness were mounted in the vessel, equipped with a Kistler 701A pressure transducer. These provided excellent optical access. Turbulence was created by four identical steel eight bladed fans, driven by four 8 kW controllable speed induction motors. The rms turbulence velocity,  $u'$ , was related to the fan speed by:

$$u' \text{ (m/s)} = 0.00119 N_f, \quad (6)$$

where  $N_f$  is the fan speed in rpm [50] Values of  $u'$  ranged from 0.6 to 9 m/s, at pressures of 0.1, 0.5, and 1.0 MPa. Temperatures were 300, 360 and 365 K. The integral length scale was found by two-point correlation to be  $0.02 \pm 0.001$  m. Two 2 kW electric heating coils, at opposite faces, provided uniform heating. About 10 explosions, under nominally identical conditions, were observed to assess the probability of continuing flame propagation,  $p_b$ .

In defining the probability of burning, a burn was an ignition attempt that resulted in complete burning, even if it was faltering and approaching extinction at some stage A quench was an ignition attempt that resulted in incomplete burning, with cessation of propagation and dissipation of the former propagating kernel. The probability of burning was the number of burns divided by the number of burns plus quenches.

Two optical techniques were employed. 2D schlieren cine photography and 3D swinging laser sheet imaging. Well time-resolved, detailed, sequences of flame quenching could only be

captured using schlieren photography. The swinging laser sheet imaging repetition frequency was a maximum of 60 kHz, too low to record fully a detailed temporal quenching sequence. In both techniques, the mixtures and turbulence were close to homogeneous and isotropic [43].

With schlieren imaging, a Lucas 12 V ignition coil provided spark energy of 23 mJ to central electrodes. With swinging sheet imaging, a New Wave solo 120 Nd:YAG ignition laser,  $I_gL$ , at a wavelength of 532 nm, with a maximum pulse repetition rate of 15 Hz, was used for ignition.

The schlieren light source was a 20 mW class 3B diode laser with a centre wavelength of 635 nm. Two plano-convex lenses,  $f = 1,000$  mm, focussed the laser beam across a knife-edge, directly onto the Miro M310 camera to capture images. The resolution was 768 x 768 pixels and the sampling rate 5400 Hz. Mie-scattered images were recorded by a high-speed digital camera, Phantom V2011 (PCC 2.7), at a frequency of 54 kHz, with an image resolution of 512 x 512 pixels. Schlieren imaging created high speed kernel 2D images. The swinging sheet, 3D, technique, although slower, revealed the kernel structure, its sphericity and volume. The volume,  $v_i$ , of each burned pixel was determined, based on the camera resolution,  $0.0075 \text{ mm}^3$ , with each pixel side measuring 0.196 mm. The total volume of the flame was the sum of these pixel volumes. The measured mean spherical diameter is,  $d_k$ . The 2D imaging gave mean, near quench, kernel diameters 9% higher than the 3D values.

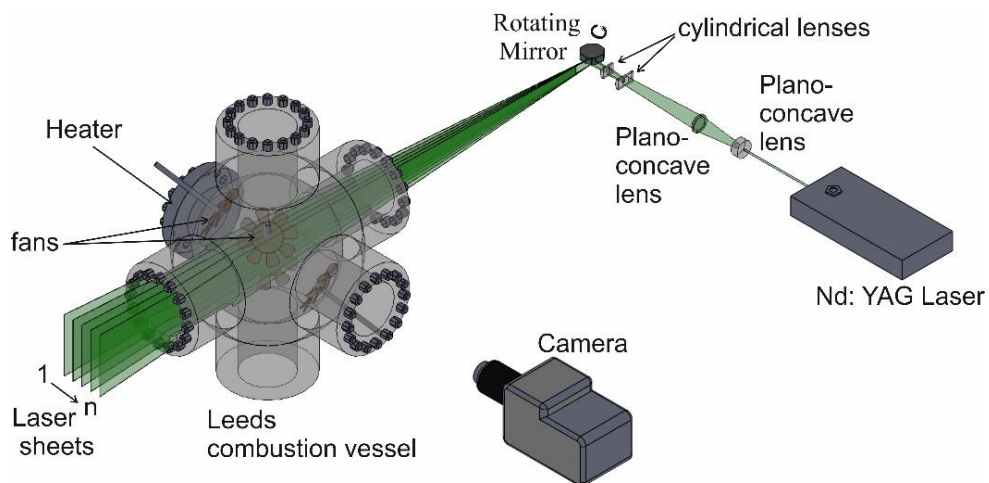


Fig. 1. Schematic diagram of the 3D swinging laser sheet system.

The swinging sheet technique [51, 52], visualised in Fig. 1, created multiple thin vertical slices of imaging laser,  $IL$ , sheets, sweeping through the propagating flame. 2D images, recorded by

a digital camera at every position, less than 1 mm apart, of the IL sheet in a single sweep were used to reconstruct the 3D flame. Olive oil, with an evaporation temperature of 570 K was used as a seed, with a typical diameter of 1.06  $\mu\text{m}$  and density of 970  $\text{kg}/\text{m}^3$  [53].

A 532 nm Nd:YAG, IL, with two internal cavities, each capable of repetition rates ranging from 5 kHz to 30 kHz, provided the pulsed light source, with pulse energies from 13 mJ to 1.9 mJ, respectively. Using double cavity staggered pulsing, a maximum laser frequency of 60 kHz could be achieved at minimal pulse energy. The beam from the IL head passed through a plano-convex lens, to focus at the centre of the bomb. Two plano-convex cylindrical lenses, with focal lengths  $f = 38.1$  and 25 mm, ahead of the 16 facets rotating mirror, RM, generated a vertically expanded IL sheet, approximately 100 mm high, across the central area of the vessel. The speed of the RM, was measured by a class 3B helium neon diode laser. This laser was pointed towards the RM, and a photo-diode detected the reflected light from the RM. For synchronizing the swinging laser sheets system, at a given IL repetition rate, the RM speed determined both the sheet spacing and the number of sweeps through each explosion. The lower the mirror speed, the closer the sheets, and lower the number of sweeps. The imaging laser, IL, and the ignition laser,  $I_{\text{g}}L$ , were pulsed at 51 up to 54 kHz and 12 Hz, respectively. Typically, 73 to 78 sheets were recorded in each sweep of 1.44 ms. This enabled an accurate 3D image of the kernel to be constructed, using MATLAB software.

To obtain equivalent diameters of schlieren image kernels, the 2D projected areas were measured, and the flame surface areas calculated from the black pixels in the binary images. The inner layer temperatures, for  $\text{CH}_4$  and  $\text{H}_2$ ,  $T^0$ , were evaluated from [46] at the different pressures. For *i*-octane,  $T^0$  was evaluated from [54]. Due to the lack of data for *n*-butanol,  $T^0$  was estimated from methanol and ethanol data [54, 55]. Equation (5) yielded  $\delta_k$ .

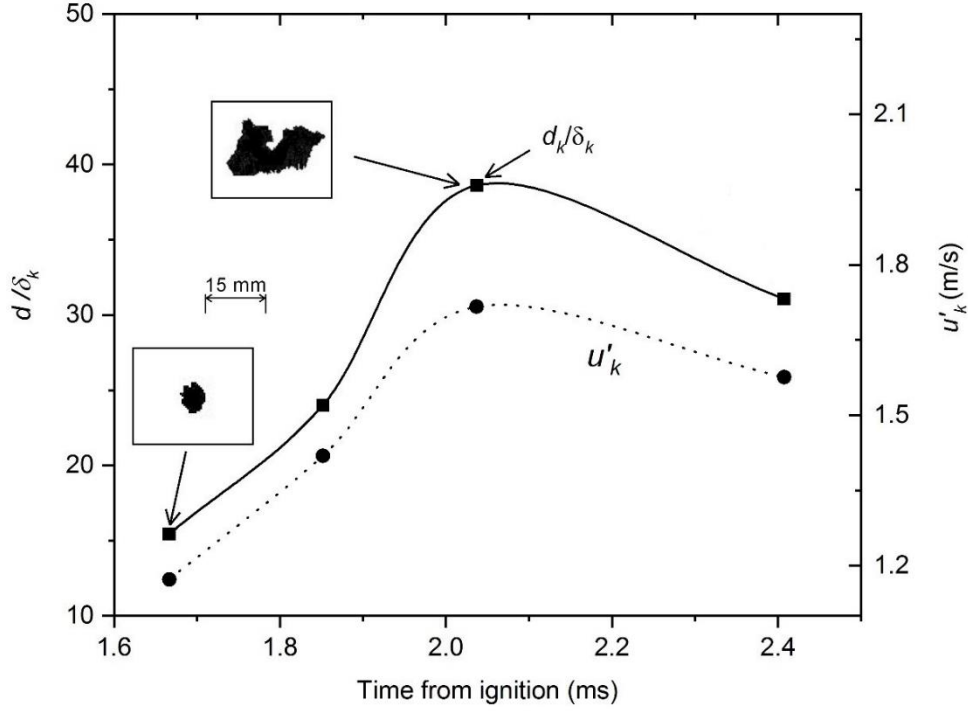


Fig. 2. Temporal variation of  $d/\delta_k$  and  $u'_k$  from ignition, for quenching of a  $\text{CH}_4/\text{air}$  kernel at 0.5 MPa and 365 K at  $\varphi=0.6$ ,  $K=11.6$ , and  $u'=4.75$  m/s.

Fragmented igniting turbulent flame kernels, diameter,  $d$ , were created that formed propagating flames exposed to increasing turbulence. This eventually quenched reaction, and the kernels were dissipated. Values of  $d$ , normalised by  $\delta_k$ , are plotted against time from ignition, in Fig. 2, for a lean  $\text{CH}_4/\text{air}$  mixture at high  $K$ . A growing kernel is shown inset, with a second at the maximum survival diameter, together with a scaling bar for 15 mm. After the mean kernel diameter has reached a maximum at a critical value,  $d_k$ , it starts to disintegrate and ultimately quench. The dotted curve of  $u'_k$ , is obtained from the measured  $u'$  and Eq. (2). Flame propagation requires normalised diameters greater than  $d_k/\delta_k$ .

In contrast, Fig. 3 shows changing values of  $d/\delta_k$  from (a) 2D schlieren, and (b) 3D swinging sheet, images for  $\text{CH}_4/\text{air}$ ,  $\varphi = 1.35$  at 365 K and 0.5 MP, for  $u' = 3$  m/s and 2 m/s, respectively, in transitions to a propagating turbulent flame. In Fig. 3(a) the earlier images reflect their electric spark origin. The five images show the initial transition from spark kernel to developing flame. A core of burned gas supports the propagating flame. It is close to quench, but it survives, at the edge of the turbulent flame regime [45] shown in Fig. 10.

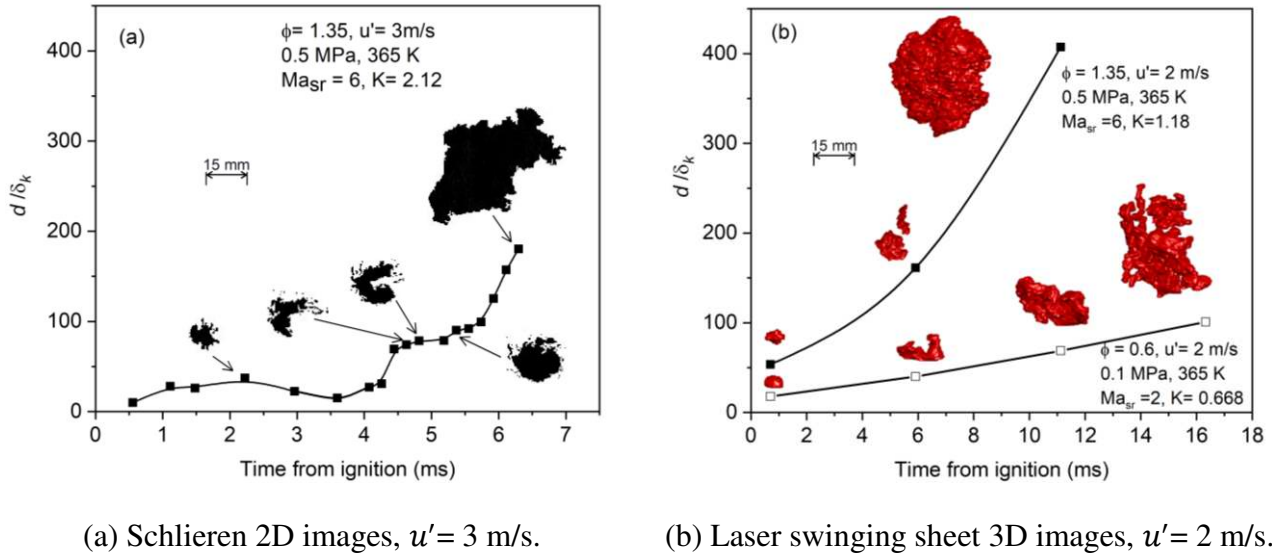


Fig. 3. Temporal variations of  $d/\delta_k$  from ignition for near-quench  $\text{CH}_4$ -air at 365 K from (a) schlieren, and (b) swinging laser sheets.

Swinging sheet images give more spatial information on the developing flame structure, close to quench, while the schlieren images give a more continuous record, on account of the shorter time interval between adjacent sheets. The 3D images clearly show, for both flames, a successful struggle for survival against the increasing turbulence as the flame develops. The lower flame kernel in Fig. 3(b) survives a broken cusp-like shape at 6 ms and indicates the developing turbulence.

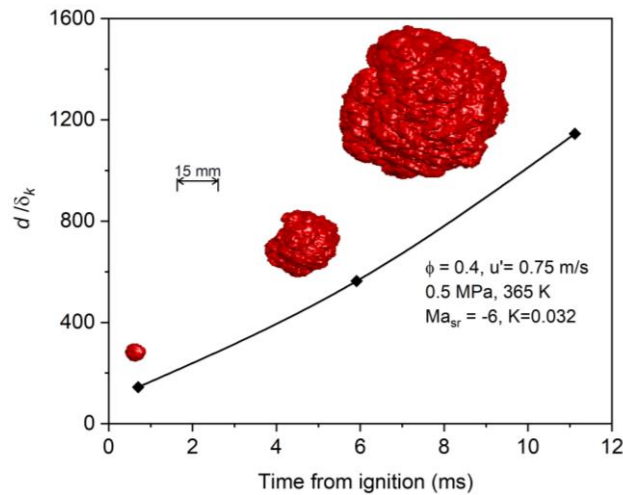


Fig. 4. Temporal variations of  $d/\delta_k$  from ignition for  $\text{H}_2$ /air at 365 K from swinging laser sheet images,  $u' = 0.75$  m/s. Mixture details on the figure.

Shown in Fig. 4 is a turbulent flame more remote from the quench regime, much less fragmentary, and more robust than the flames in Fig. 3. The flame speed is significantly higher.

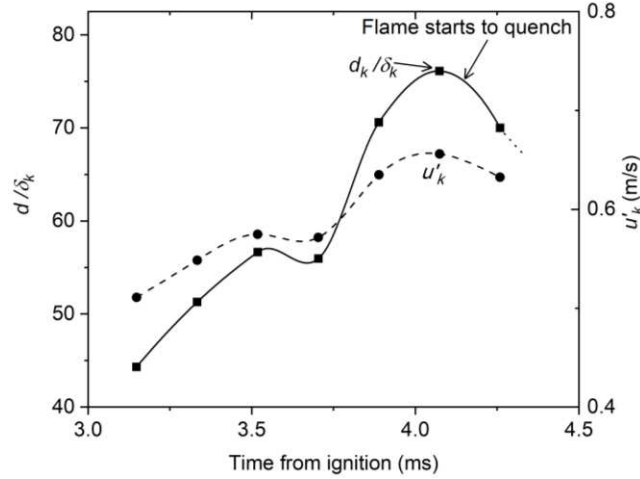


Fig. 5. Temporal variations of  $d/\delta_k$  and  $u'_k$  with time from ignition for  $n$ -butanol/air at 360 K, 0.5 MPa,  $\varphi = 0.7$  and  $u' = 2$  m/s,  $K = 0.478$ ,  $p_{0.4}$ .

In Fig. 5, the  $d/\delta_k$  traces at  $u' = 2$  m/s, for  $n$ -butanol/air from schlieren images, are of interest, in that the kernel is about to extinguish at  $d/\delta_k = 55$ . The propagation then revives, but extinction finally occurs at  $d_k/\delta_k = 77$ .

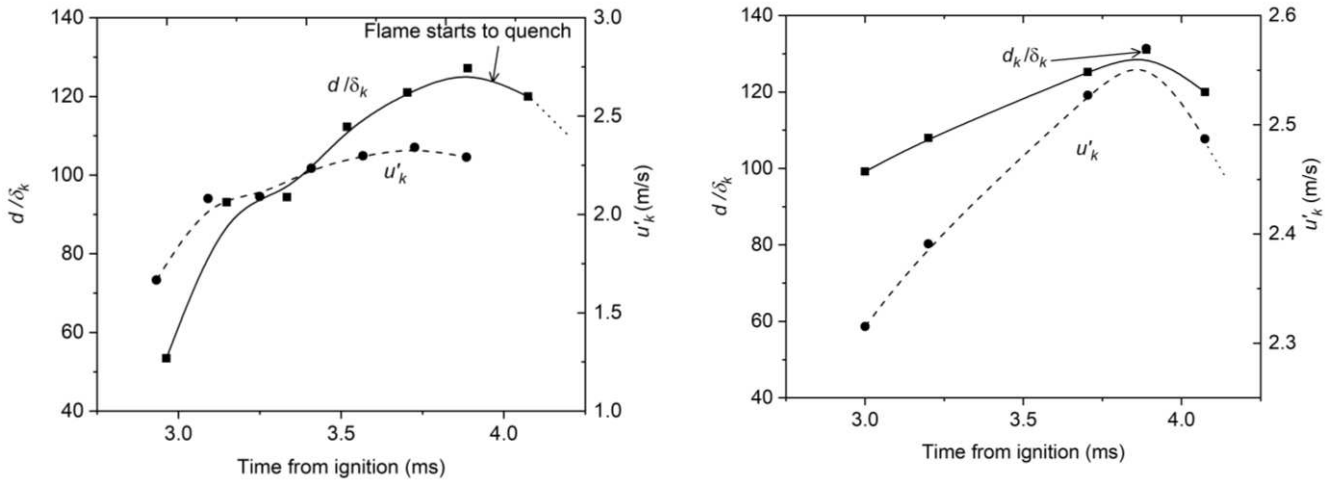


Fig. 6. Two contrasting temporal variations of  $d/\delta_k$  and  $u'_k$  with the same  $i$ -C<sub>8</sub>H<sub>18</sub>/air mixtures at 365 K, 0.5 MPa,  $\varphi = 0.8$  and  $u' = 6$  m/s,  $K = 1.34$ , with  $p_{0.6}$ .

Figure 6 is of interest in showing how, for nominally the same conditions, the temporal profiles of  $d/\delta_k$  can be very different, yet yield similar ultimate values of  $d_k/\delta_k$ . The stretch rate was never sufficient to cause extinction of the initial small flame fragments. The kernel always grew, becoming increasingly spherical, eventually reaching the critical size, at which the combination of flame stretching and developing turbulence quenched it.

In Fig. 7, although combustion of  $H_2$  appears to be the most rapid, this is because of the small values of  $\delta_k$ . The hydrogen flame fragments were smaller and took longer to disappear than those of  $CH_4$ .

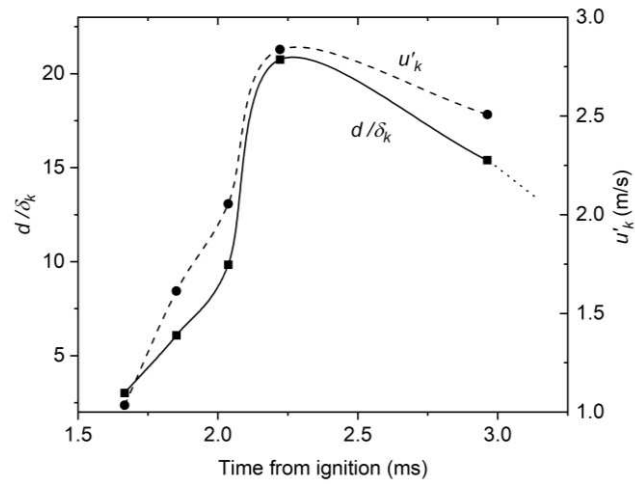


Fig. 7. Temporal variation of  $d/\delta_k$  for  $H_2/0.11 O_2/0.89 N_2$  mixtures at 300 K, 0.1 MPa,  $\varphi = 0.5$  and  $u' = 7$  m/s,  $K = 14.4$ , with  $p_{0.6}$ .

Table 1. Experimental Quench Data

Fuel/air mixture	Method	$T$ (K)	$P$ (MPa)	$\varphi$	$u'$ (m/s)	$u'_k$ (m/s)	$\frac{d_k}{\delta_k}$	$T^o$ (K)	$u_l$ (m/s)	$\nu$ (m <sup>2</sup> /s)	$K$	$Ma_{sr}$	$Ka$	$p_b$
H <sub>2</sub> /0.11 O <sub>2</sub> /0.89 N <sub>2</sub>	Schlieren system	300	0.1	0.5	6	2.14	16	1003	0.0975	1.76E-05	11.46	0.03	48	0.8
H <sub>2</sub> /0.115 O <sub>2</sub> /0.885 N <sub>2</sub>		300	0.1	0.5	7	3.062	17	1003	0.111	1.77E-05	11.284	-0.1	46	0.8
H <sub>2</sub> /0.11 O <sub>2</sub> /0.89 N <sub>2</sub>		300	0.1	0.5	7	2.8	21	1003	0.0975	1.76E-05	14.445	0.03	58.6	0.6
H <sub>2</sub> /0.118 O <sub>2</sub> /0.882N <sub>2</sub>		300	0.1	0.5	9	3.38	23	1003	0.124	1.77E-05	13.14	-0.4	53.28	0.8
H <sub>2</sub> /air		365	0.5	0.15	2.25	0.82	24	1172	0.036 [11]	4.79E-06	10.075	-2 [11]	39.71	0.8
<i>n</i> -C <sub>4</sub> H <sub>10</sub> O/air		360	1	0.7	0.6	0.121	62	1500	0.095	2.14E-6	0.1215	6	0.388	0.8
<i>n</i> -C <sub>4</sub> H <sub>10</sub> O/air		360	0.5	0.7	2	0.66	76	1400	0.147	4.27E-06	0.4785	9	1.89	0.4
<i>n</i> -C <sub>4</sub> H <sub>10</sub> O/air		360	0.5	0.7	2	0.61	80	1400	0.147	4.27E-06	0.4785	9	1.89	0.4
<i>i</i> -C <sub>8</sub> H <sub>18</sub> /air		365	0.5	0.8	6	2.3	125	1320	0.201[11]	4.37E-06	1.344	5 [11]	5.47	0.6
<i>i</i> -C <sub>8</sub> H <sub>18</sub> /air		365	0.5	0.8	6	2.34	127	1320	0.201 [11]	4.37E-06	1.344	5 [11]	5.47	0.6
<i>i</i> -C <sub>8</sub> H <sub>18</sub> /air		365	0.5	0.8	6.5	2.57	131	1320	0.201[11]	4.37E-06	1.516	5 [11]	6.51	0.4
CH <sub>4</sub> /air		365	0.5	1.35	3	0.83	37	1328	0.095 [11]	4.60E-06	2.183	6 [11]	8.54	0.8
CH <sub>4</sub> /air	Swinging sheets System	365	0.1	0.6	2	0.588	22	1220	0.189 [11]	2.28E-5	0.668	2 [11]	2.65	0.9
CH <sub>4</sub> /air		365	0.1	0.6	2	0.6	24	1220	0.189 [11]	2.28E-5	0.668	2 [11]	2.65	0.9
CH <sub>4</sub> /air		300	0.1	1.3	2	0.64	25	1220	0.16 [10]	1.63E-05	0.788	4 [10]	3.068	0.8
CH <sub>4</sub> /air		300	0.1	1.3	2	0.69	32	1220	0.16 [10]	1.63E-05	0.788	4 [10]	3.068	0.8
CH <sub>4</sub> /air		365	0.5	1.35	2	0.728	68	1328	0.095 [11]	4.60E-06	1.1882	6 [11]	5.06	0.8
CH <sub>4</sub> /air		365	0.5	1.35	2	0.74	77	1328	0.095 [11]	4.60E-06	1.1882	6 [11]	5.06	0.8

### 3. The Quenched Flame Regime and Jet Flame Blow-off

#### 3.1 Generalised approach

The generality of turbulent combustion is emphasised by combining the present data on premixed flame quenching diameters,  $d_k/\delta_k$ , with those for lifted jet flame pipe diameters at blow-off,  $D_b/\delta_k$ , from [56]. The fuel jet flow rate in [56] is characterised by a dimensionless flow number,  $U^* = (u/u_{lm})(\delta_k/D)^{0.4}(P_i/P_a)$ . Values of  $U^*$  at blow-off are  $U_b^*$ . Here the jet flow number at blow off,  $U_b^*$ , has similarities with  $K$ . These similarities with  $D_b/\delta_k$  are well characterised in the combined plot of  $d_k/\delta_k$  against  $K$ , and  $D_b/\delta_k$  against  $U_b^*$  in Fig. 8.

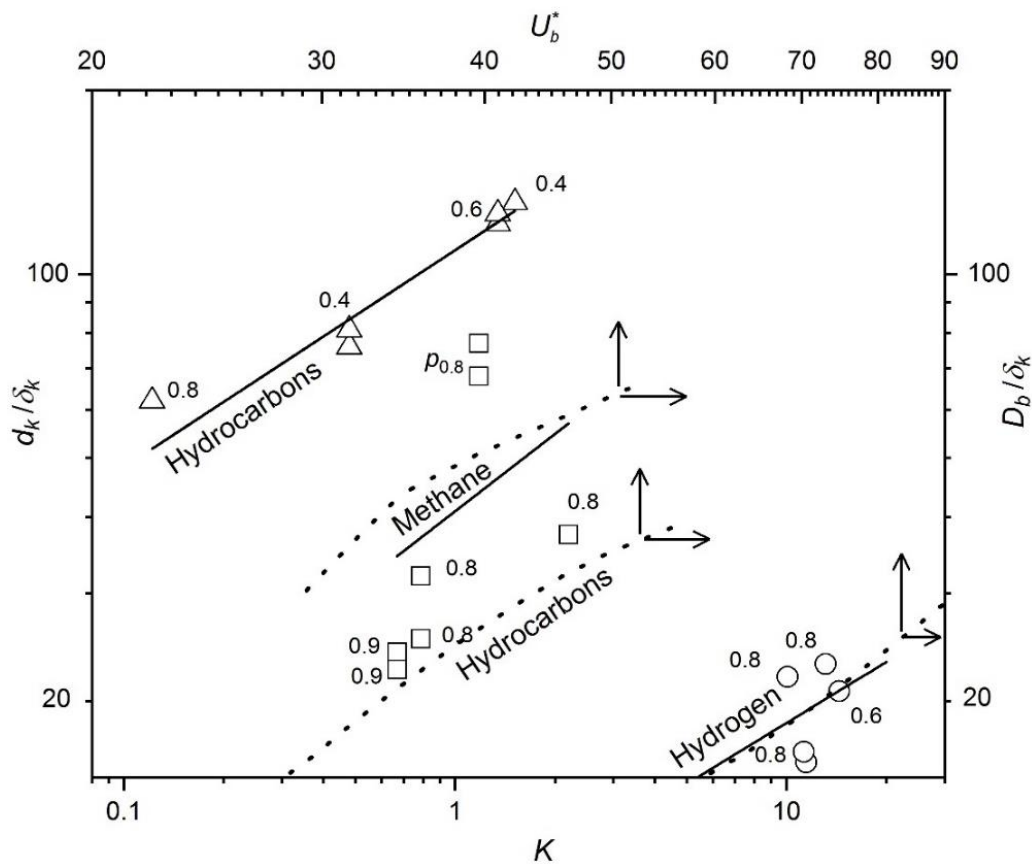


Fig. 8. Variations of Kernel and Burner Quenching Distances with Flow Rates.

Premixed turbulent flames only exist above full lines. Turbulent jet flames only exist above dotted lines. Symbols:  $\triangle$ , for hydrocarbons,  $\square$ , for  $\text{CH}_4$ , and,  $\circ$ , for  $\text{H}_2$ , throughout paper.

Numbers adjacent to symbols are  $p_b$  values.

#### 3.2. Quenching of premixed flame kernels

All the experimental data on  $d_k/\delta_k$  are listed in Table 1. Fig. 8 shows the inter-relationships with jet flame key parameters. Values of  $Ka$  also are given in Table 1. Premixed flame kernels

decay below the full lines. Above them, are propagating flames. The limit values of  $d_k/\delta_k$  increase with  $K$ . The grouping of the higher hydrocarbons, is listed in Table 1. The same unique symbols are used for each fuel category throughout the paper. The hydrocarbons display similar values of  $d_k/\delta_k$ , although they are more conveniently correlated in terms of  $p_{0.4}$ . The hydrocarbons are the most easily quenched, at the lowest values of  $K$ , and are associated with the highest values of  $Ma_{sr}$ . Hydrogen mixtures are the most difficult to quench, at the highest values of  $K$ , and are associated with the lowest and negative values of  $Ma_{sr}$ . Methane mixtures have intermediate  $Ma_{sr}$  values. It should be noted that  $Ma_{sr}$  values have relatively large error bands [57].

The fragmentary flames in the quench regime in Figs. 3 to 7, propagate with increasing localised turbulence,  $u'_k$ . Overall, flame speeds are low, increase with  $K$ , and the kernel diameters increase, prior to quench. Flame speeds are appreciably lower for hydrogen flame kernels and this probably explains the relatively low  $d_k/\delta_k$  values.

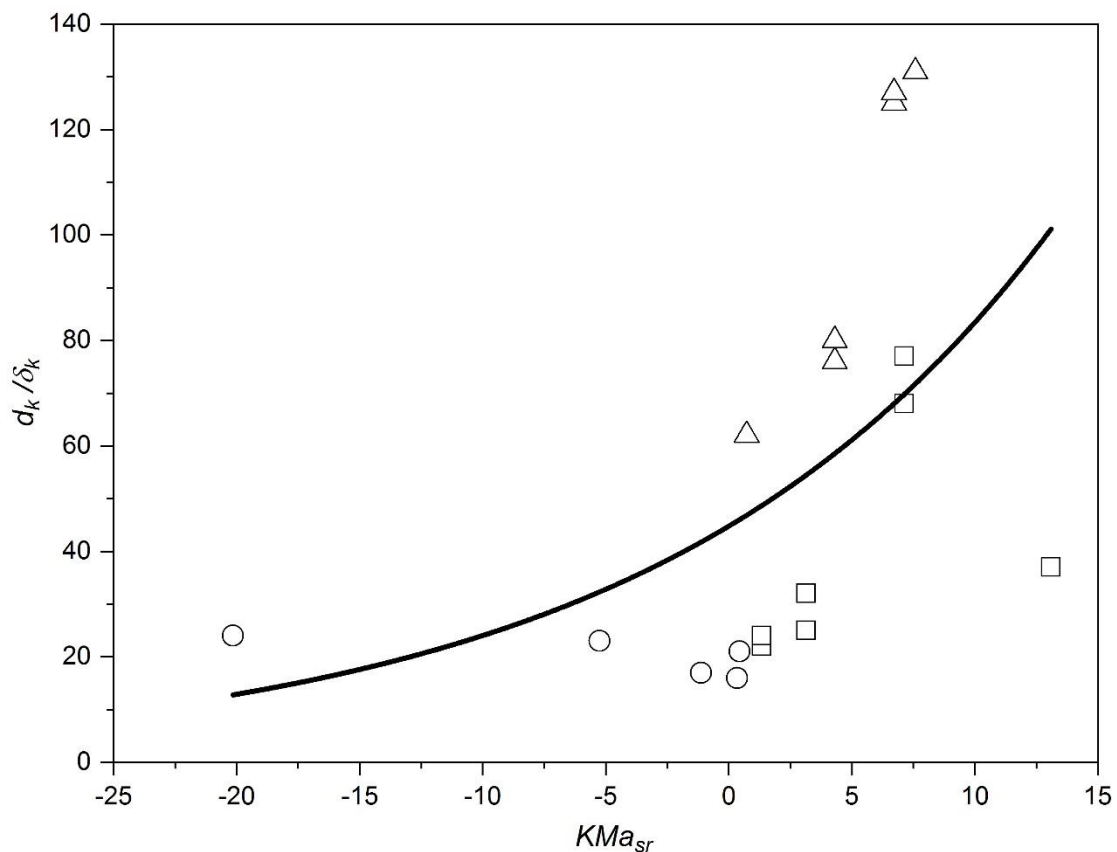


Fig. 9. Values of  $d_k/\delta_k$  for different  $KMa_{sr}$  at flame quench. See Fig. 8 for symbols key.

Normalised flame kernel sizes at flame extinction correlate with  $K$ , and, to a degree, also  $Ma_{sr}$ . Figure 9 shows  $d_k/\delta_k$  plotted against  $KMa_{sr}$ , an increase in which is normally indicative of an increase in burn rate up to quench. This would perhaps explain the increases in  $d_k/\delta_k$  with  $KMa_{sr}$ .

### 3.3 Quenching of lifted jet flames

Turbulent lifted fuel jet flames entrain air, and the leading reaction zone is the most reactive region, where the local mixture attains that of the maximum laminar burning velocity,  $u_{lm}$ , [58]. Thereafter, with increasing fuel jet velocity,  $u$ , more air is entrained and its reaction with the fuel is aided by the mixing with the hot gases created in the initial most reactive zone. Eventually the jet entrains more than sufficient air for reaction, the flame quenches, and blows off the burner. For a given fuel jet velocity, pipe diameters, less than the critical size,  $D_b$ , that cannot maintain a flame and blow-off occurs.

Jet flames only exist above the dotted lines. From its derivation, it is apparent that  $U^*$  has a similarity with  $K$  [37, 56].  $U_b^*$  therefore, appears as the secondary  $x$ -axis, against which the present experimental values of  $D_b/\delta_k$ , on the secondary  $y$ -axis, are plotted by the dotted lines. For both  $CH_4$  and hydrocarbons, choked jet flow, develops above about  $U^* = 200$ .

Although the limiting values of  $d_k/\delta_k$  and  $D_b/\delta_k$  in the two sets of diverse results are rather different, they reflect the underlying similarity between premixed and jet flamelet structures. A striking aspect of both sets of curves is the sharp increases in  $d_k/\delta_k$  and  $D_b/\delta_k$  with  $K$  and  $U_b^*$ , respectively. Furthermore, both sets of normalised diameters decrease with  $Ma_{sr}$ . For  $H_2$ , both sets of values exist over greater ranges of  $K$  and  $U_b^*$  than is the case for other fuels. This implies that large increases in  $u'$  and  $u$  can create high burning rates, only if they are accompanied by large commensurate increases in, respectively, explosion vessel sizes and burner diameters. The role of  $KMa_{sr}$  is important in controlling both burn rate [59] and quench. Figure 9 shows its influence upon quenching kernel size, with  $d_k/\delta_k$  increasing with  $KMa_{sr}$ . Quenching distances dominate the relationships in Figs. 8 and 9. The quenching of turbulent burning velocities is now examined.

## 4. The Turbulent Flame Regime

The regime of turbulent flame quenching and normalised turbulent burning velocity,  $U$ , in [44] was re-examined in the light of the data in [11] and Table 1. A new correlation of  $U$ ,  $K$  and  $Ma_{sr}$  for quenching is proposed. Data have been taken from the current work and from [11],

based on  $p_{0.8}$  for the different mixtures. It was found that the influences of  $Ma_{sr}$  and  $K$  on quench could be expressed through the relationship:

$$Ma_{sr} = -2.24 \ln(K) + 3.8. \quad (7)$$

Not surprisingly, the quenching tendency increases with  $K$ , at the larger values of which, negative values of  $Ma_{sr}$  become necessary for flame survival. No flame quenching was observed for  $H_2/air$  at  $Ma_{sr} = -2.8$  [11], even when  $u'$  was increased to 10 m/s, the maximum attainable value. This imposed a limit, with no data being available on flame quenching for  $Ma_{sr} < -2$ . This new correlation contributes to the revised form of  $U/K$  diagram, shown in Fig. 10.

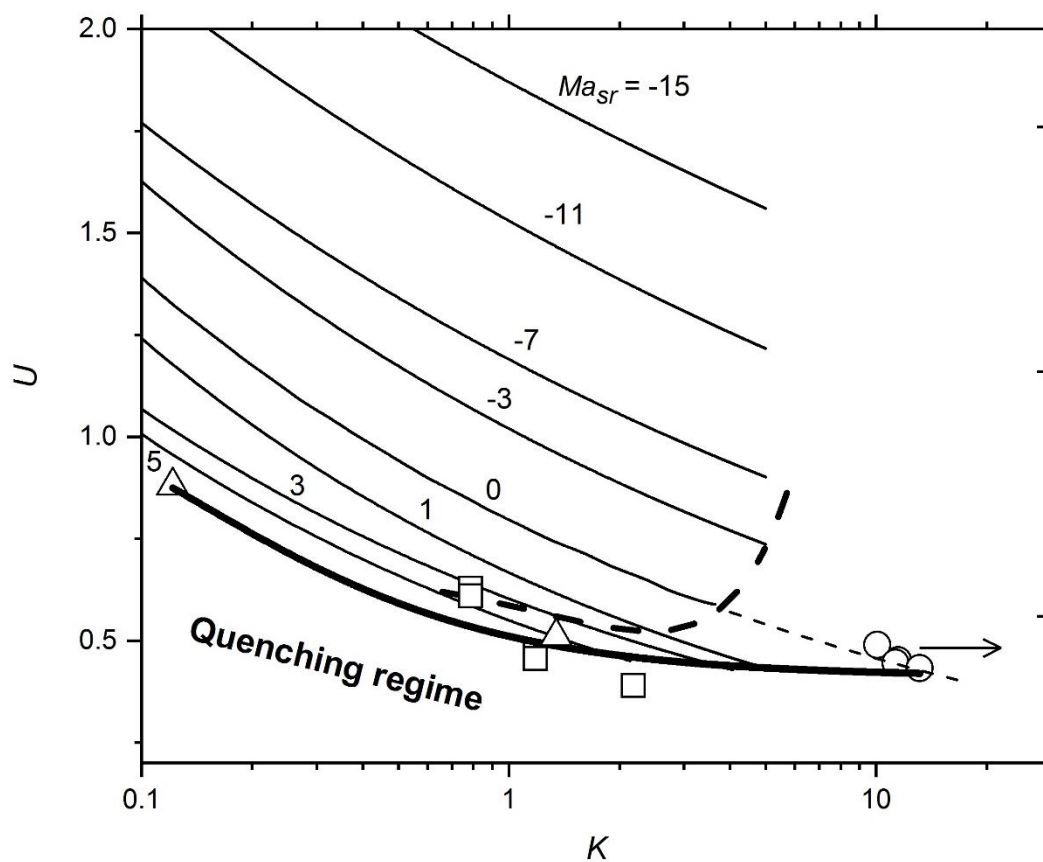


Fig. 10.  $U/K$  diagram of turbulent combustion, including the new limits of quenching for  $p_{0.8}$ , shown by the bold curve. Dashed curve is the former flame quench boundary, in [44]. Symbols show current experimental points.

The quenching limits extend beyond the previous limit [45], shown by the dashed curve, and  $p_{0.8}$  is expressed by the bold curve in Fig. 10, the new quenching regime boundary. In addition to the influences of the new correlations, expressed in Eq. (7), due regard was paid to the observed sustainability of near-marginal flames, such as those in Fig. 3, in constructing the

curve for the onset of quenching. Since  $U$  is a function of  $Ma_{sr}$  and  $K$ , the best fit curve presented in Eq. (7) should also hold good for the quench limit shown by the solid line in Fig. 10. The quench regime now covers higher values of  $K$  and  $Ma_{sr}$  than previously. Using the  $Ma_{sr}/K$  correlation, the  $Ma_{sr}$  values for different  $K$  from Eq.(7), were used to calculate  $U$  values for different  $K$ . The equations given in [44] and [45] were employed:

$$U = \alpha K^\beta, \text{ for } -23 \leq Ma_{sr} \leq 5, \quad (8)$$

where  $\alpha$  and  $\beta$  are constants in terms of  $Ma_{sr}$  given in [45].

### 5. Premixed flames supported by annular pilot flames

Some of the similarities between premixed and jet flame combustion are relevant to the important studies of Wabel et al. [60] of highly turbulent premixed flames, supported by a pilot flame. Their configuration involved lean turbulent mixtures close to quench in a main premixed burner, with a surrounding pilot flame. Just as a fuel jet flame is sustained through the entrainment of surrounding air, such a main turbulent flame is sustained by entrainment of pilot flame gases.

In the configuration employed in [61] both main and pilot burner entry mixture compositions were identical, and were comprised of  $CH_4/air$ ,  $\varphi = 0.75$ , at atmospheric pressure, and 298K, with  $u_l = 0.23$  m/s. Three different operational flow modes, here listed as, A, B, and C. were studied and the values of  $u'$  and  $L$ , taken from [60], appear in Table 2(a). Along with the values of  $u_l$  for  $CH_4/air$  at  $\varphi = 0.75$ , values of  $K$  were found from Eq. (1), and these are given in Table 2(a). The minimum value of  $K$  is 20.9. With an estimated value of  $Ma_{sr} = 2.7$  [62], it is clear from the quenching regime boundary in Fig. 10 that, were there to be no pilot flame under the given conditions, this flame would have quenched.

Table 2: Effect of different fractions of pilot flame entrainments on  $K$  values, for Hi-pilot burner in [60].

2(a) Michigan Hi-pilot burner ( $\varphi = 0.75$ ) [60]						2(b) $K$ values from Model [61] ( $\varphi = 0.75$ )		
Mode	$u'$ (m/s)	$L$ (mm)	$R_L$	$u$ (m/s)	Burner $K$	$f=0.1$	$f=0.2$	$f=0.3$
A	37	41	99,000	78	20.9	8.06	3.95	2.21
B	29	12	22,300	72	27.1	10.34	5.06	2.84
C	38	17	40,900	89	33.3	13.0	6.37	3.57

A simple model that assumes different mass fractions,  $f$ , of burned gas in a mixture with the reactants, was employed to demonstrate effectiveness of a pilot flame. It is assumed that the burned flame gases of the pilot flame become perfectly mixed with the unburned mixture within the main burner. The temperature of the resulting mixture will be high, and provided the effect of the enhanced temperature in increasing burning velocity overcomes the deleterious effect of mixture dilution by burned gas, then the combustion will be enhanced.

In this context, Sidey et al. [61], have performed relevant computations for different CH<sub>4</sub>/air values of  $\varphi$  and different proportions of burned to unburned mixture. Mixture burning velocities,  $u_l$ , were also computed for the resulting adiabatic mixtures, at their respective adiabatic temperatures, using the Chemkin Code [63]. These data were used in the present study, with some cross-plotting for different  $\varphi$ . Results of the calculations are presented in Table 3 for three different mass fractions,  $f$ , of burned gas, namely  $f = 0.1, 0.2,$  and  $0.3$  for CH<sub>4</sub>/air  $\varphi = 0.75$ , at atmospheric pressure.

Table 3. Final adiabatic mixture temperatures,  $T_u$ , and associated values of  $u_l$  for three different burned gas mass fractions  $f$ .

$f$	$T_u$ (K)	$u_l$ (m/s)
0.1	489	0.46
0.2	668	0.75
0.3	837	1.1

With further increase in  $f$ ,  $u_l$  eventually falls, but, as can be seen, initially the temperature increases of the original mixtures increase the  $u_l$  values of the mixture to a greater extent than the dilutions with burned gas decrease them. These adiabatic mixture values of  $u_l$  for the three values of  $f$ , when combined with the values of  $u'$  and  $L$  for the three operational modes in Table 2(a), yield the operational  $K$  values for the three values of  $f$  given in Table 2(b). These  $K$  values are based on the more realistic higher values of  $u_l$ , that yield noticeably lower  $K$  values than those in Table 2 (a), particularly at the highest value of  $f$ . Of course, the burner mixtures' entrainment of pilot flame gases is more complex than is the mixing in the present model, but nevertheless the significantly lower values of  $K$  in Table 2(b), than those for the Burner in Table 2(a), illustrate the general principle of how main flame quenching is ameliorated.

The main burner entry values of  $K$  in Table 2(a), are high enough to suggest, from Fig. 10 that all the flames would be quenched. However, when allowance is made for pilot flame entrainment, for those with  $f = 0.2$  and  $0.3$ , the  $K$  values suggest they could avoid quench at the estimated value of  $Ma_{sr}$  of 2, although, for  $f = 0.1$ , flames would be more vulnerable. The pilot flame would ensure normal flame propagation could occur.

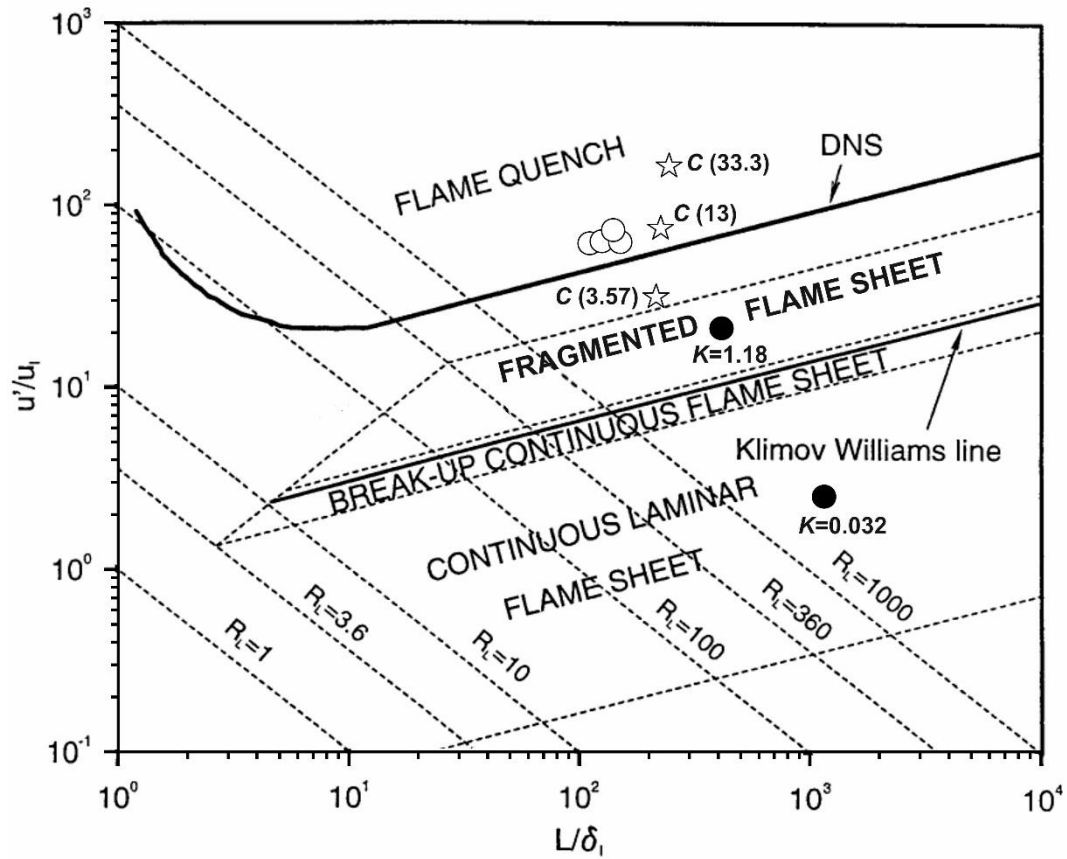


Fig. 11. Extended Borghi diagram [36] with DNS curve is from [35]. Data points from three sources: Pilot flame burner, ☆, ●, swinging sheet, ○, near-quench  $H_2$  with  $p_{0.8}$ .

It is fruitful to employ the extended Borghi diagram from [36], to identify the combustion regimes of some of these diverse operational points from the pilot flame burner. The three stars in Fig. 11 identify the highest levels of turbulence in operational Mode C of the burner at the highest  $K$  value of 33.3. With the associated values of  $u'/u_l$  and  $L/\delta_l$ , this point is identified by the (C33.3) star point in Fig. 11. It is well into the flame quench regime. With the calculated amelioration of the entrained pilot flame gas, with  $f = 0.1$  the calculated value of  $K$  is 13.0. On Fig. 11 this is identified by (C13), just into the flame quench regime. However, with  $f = 0.3$ , the calculated value of  $K$  of 3.57, (C3.57), but no longer in the quench regime.

Also shown in Fig. 11 are two sets of conditions from the present experiments. One, for  $K = 1.18$ , shows the turbulent flame conditions recorded by the swinging sheet in the upper part of Fig. 3(b). A lower point, for  $K = 0.032$ , is for the swinging sheet flame, more remote from quench, in Fig. 4. Finally, the near-quench,  $H_2 p_{0.8}$  flames, in Fig. 10, are re-plotted, by four open circle symbols, to show their proximity to the quench line of Poinso et al. [35].

## 5. Conclusions

- (a). Experimental data, from a fan-stirred, explosion sphere, have extended the boundary of the previously defined regime, within which stable premixed turbulent combustion occurs, see Fig. 10. The regime of evaluations was limited by the maximum value of  $u' = 10$  m/s.
- (b). New experimental data on the flame kernel normalised diameters that are necessary for the attainment of a propagating turbulent flame, show  $d_k/\delta_k$ , to increase with  $K$ , and decrease with  $Ma_{sr}$ , in Fig. 8.
- (c). There are informative parallels between  $d_k/\delta_k$ , and  $D_b/\delta_k$ , the normalised fuel jet pipe diameter with flame extinction, at blow-off.
- (d). For lifted jet flames,  $D_b/\delta_k$ , increases with  $U^*$  and decreases with  $Ma_{sr}$ , see Fig. 8.
- (e). For hydrogen, values of  $d_k/\delta_k$ , and  $D_b/\delta_k$ , are possible over greater ranges of conditions than for other fuels.
- (f). It has been demonstrated how entrainment of pilot flame gases prevents extinction of highly turbulent premixed flames.
- (g). Structures of both turbulent flames, and quenching kernels, have been revealed by the swinging laser sheet technique.

## Acknowledgements

M.S. is grateful to the Egyptian Cultural and Educational Bureau and Port Said University for their financial support. P.A. thanks the University of Leeds for a Research Scholarship Award.

## References

- [1] J.M. Donbar, J.F. Driscoll, C.D. Carter, Strain rates measured along the wrinkled flame contour within turbulent non-premixed jet flames, *Combust. Flame* 125 (2001) 1239-1257.

- [2] C.K. Law, S. Ishizuka, M. Mizomoto, Lean-limit extinction of propane/air mixtures in the stagnation-point flow, *Symp. (Int.) Combust.* 18 (1981) 1791-1798.
- [3] C. Law, D. Zhu, G. Yu, Propagation and extinction of stretched premixed flames, *Symp. (Int.) Combust.* 21 (1988) 1419-1426.
- [4] S. Yang, S. Shy, Global quenching of premixed CH<sub>4</sub>/air flames: Effects of turbulent straining, equivalence ratio, and radiative heat loss, *Proc. Combust. Inst.* 29 (2002) 1841-1847.
- [5] C. Ji, E. Dames, Y.L. Wang, H. Wang, F.N. Egolfopoulos, Propagation and extinction of premixed C<sub>5</sub>–C<sub>12</sub> n-alkane flames, *Combust. Flame* 157 (2010) 277-287.
- [6] J. Chomiak, J. Jarosiński, Flame quenching by turbulence, *Combust. Flame* 48 (1982) 241-249.
- [7] M. Kuznetsov, V. Alekseev, A. Bezmelnitsyn, W. Breitung, S. Dorofeev, I. Matsukov, A. Vesper, Y. Yankin, Effect of obstacle geometry on behaviour of turbulent flames, Report FZKA-6328, Karlsruhe, Forschungszentrum Karlsruhe GmbH, Karlsruhe, (1999).
- [8] P. Thibault, Y. Liu, C. Chan, J. Lee, R. Knystautas, C. Gurap, B. Hjertager, K. Fuhre, Transmission of an explosion through an orifice, NASA STI/Recon Technical Report N 83 (1982).
- [9] R. Abdel-Gayed, D. Bradley, M. Lawes, Turbulent burning velocities: a general correlation in terms of straining rates, *Proc. R. Soc. Lond. A* 414 (1987) 389-413.
- [10] D. Bradley, P. Gaskell, X. Gu, Burning velocities, Markstein lengths, and flame quenching for spherical methane-air flames: a computational study, *Combust. Flame* 104 (1996) 176-198.
- [11] D. Bradley, M. Lawes, K. Liu, R. Woolley, The quenching of premixed turbulent flames of iso-octane, methane and hydrogen at high pressures, *Proc. Combust. Inst.* 31 (2007) 1393-1400.
- [12] K. Al-Khishali, D. Bradley, S. Hall, Turbulent combustion of near-limit hydrogen-air mixtures, *Combust. Flame* 54 (1983) 61-70.
- [13] G. Dixon-Lewis, Structure and extinction limits of some strained premixed flames, Dynamics of reactive systems. Part I. Flames, *Prog. Astronaut. Aeronaut.* 113 (1988) 166-183.
- [14] R.J. Kee, J.A. Miller, G.H. Evans, G. Dixon-Lewis, A computational model of the structure and extinction of strained, opposed flow, premixed methane-air flames, *Symp. (Int.) Combust.* 22 (1989) 1479-1494.
- [15] G. Stahl, J. Warnatz, Numerical investigation of time-dependent properties and extinction of strained methane and propane-air flamelets, *Combust. Flame* 85 (1991) 285-299.

- [16] A. Holley, Y. Dong, M. Andac, F. Egolfopoulos, Extinction of premixed flames of practical liquid fuels: Experiments and simulations, *Combust. Flame* 144 (2006) 448-460.
- [17] Y. Dong, A.T. Holley, M.G. Andac, F.N. Egolfopoulos, S.G. Davis, P. Middha, H. Wang, Extinction of premixed H<sub>2</sub>/air flames: Chemical kinetics and molecular diffusion effects, *Combust. Flame* 142 (2005) 374-387.
- [18] Y. Wang, A. Holley, C. Ji, F. Egolfopoulos, T. Tsotsis, H. Curran, Propagation and extinction of premixed dimethyl-ether/air flames, *Proc. Combust. Inst.* 32 (2009) 1035-1042.
- [19] O. Park, P.S. Veloo, N. Liu, F.N. Egolfopoulos, Combustion characteristics of alternative gaseous fuels, *Proc. Combust. Inst.* 33 (2011) 887-894.
- [20] P.S. Veloo, Y.L. Wang, F.N. Egolfopoulos, C.K. Westbrook, A comparative experimental and computational study of methanol, ethanol, and n-butanol flames, *Combust. Flame* 157 (2010) 1989-2004.
- [21] Y.L. Wang, P.S. Veloo, F.N. Egolfopoulos, T.T. Tsotsis, A comparative study on the extinction characteristics of non-premixed dimethyl ether and ethanol flames, *Proc. Combust. Inst.* 33 (2011) 1003-1010.
- [22] F. Egolfopoulos, Geometric and radiation effects on steady and unsteady strained laminar flames, *Symp. (Int.) Combust.* 25 (1994) 1375-1381.
- [23] F.N. Egolfopoulos, C.S. Campbell, Unsteady counterflowing strained diffusion flames: diffusion-limited frequency response, *J. Fluid Mech.* 318 (1996) 1-29.
- [24] C.K. Westbrook, W.J. Pitz, P.R. Westmoreland, F.L. Dryer, M. Chaos, P. Oßwald, K. Kohse-Höinghaus, T.A. Cool, J. Wang, B. Yang, A detailed chemical kinetic reaction mechanism for oxidation of four small alkyl esters in laminar premixed flames, *Proc. Combust. Inst.* 32 (2009) 221-228.
- [25] S.M. Sarathy, M.J. Thomson, C. Togbé, P. Dagaut, F. Halter, C. Mounaim-Rousselle, An experimental and kinetic modeling study of n-butanol combustion, *Combust. Flame* 156 (2009) 852-864.
- [26] A. Holley, Y. Dong, M. Andac, F. Egolfopoulos, T. Edwards, Ignition and extinction of non-premixed flames of single-component liquid hydrocarbons, jet fuels, and their surrogates, *Proc. Combust. Inst.* 31 (2007) 1205-1213.
- [27] D. Bradley, Fundamentals of lean combustion, *Lean Combustion*, Elsevier 2008, pp. 19-II.
- [28] A. Klimov, *Zhournal Prikladnoi Mekhaniki i Tekhnicheskoi Fiziki* 3 (1963) 49.

- [29] F. Williams, A review of some theoretical considerations of turbulent flame structure, AGARD Conference, 164, (1975).
- [30] V. Kuznetsov, Limiting laws of propagation of a turbulent flame, *Combust. Explos. Shock Waves* 18 (1982) 172-179.
- [31] R. Abdel-Gayed, D. Bradley, F.-K. Lung, Combustion regimes and the straining of turbulent premixed flames, *Combust. Flame* 76 (1989) 213-218.
- [32] S. Shy, S. Yang, W. Lin, R. Su, Turbulent burning velocities of premixed CH<sub>4</sub>/diluent/air flames in intense isotropic turbulence with consideration of radiation losses, *Combust. Flame* 143 (2005) 106-118.
- [33] C. Liu, S. Shy, Y. Dong, M. Peng, More on global quenching of premixed CH<sub>4</sub>/diluent/air flames by intense near-isotropic turbulence, *Combust. Sci. Technol.* 184 (2012) 1916-1933.
- [34] C. Meneveau, T. Poinso, Stretching and quenching of flamelets in premixed turbulent combustion, *Combust. Flame* 86 (1991) 311-332.
- [35] T. Poinso, D. Veynante, S. Candel, Quenching processes and premixed turbulent combustion diagrams, *J. Fluid Mech.* 228 (1991) 561-606.
- [36] D. Bradley, P. Gaskell, X. Gu, M. Lawes, M. Scott, Premixed turbulent flame instability and NO formation in a lean-burn swirl burner, *Combust. Flame* 115 (1998) 515-538.
- [37] F. Williams, *Combustion Theory* 2nd, The Benjamin/Cummings 1985.
- [38] K. Bray, *Topics in Applied Physics*, PA Libby and FA Williams ed, Springer Verlag 1980.
- [39] P. Yeung, S. Girimaji, S. Pope, Straining and scalar dissipation on material surfaces in turbulence: implications for flamelets, *Combust. Flame* 79 (1990) 340-365.
- [40] D. Bradley, P. Gaskell, A. Sedaghat, X. Gu, Generation of PDFs for flame curvature and for flame stretch rate in premixed turbulent combustion, *Combust. Flame* 135 (2003) 503-523.
- [41] D. Bradley, M. Lawes, M.S. Mansour, Correlation of turbulent burning velocities of ethanol-air, measured in a fan-stirred bomb up to 1.2MPa, *Combust. Flame* 158 (2011) 123-138.
- [42] D. Bradley, M. Lawes, M.S. Mansour, Flame surface densities during spherical turbulent flame explosions, *Proc. Combust. Inst.* 32 (2009) 1587-1593.
- [43] D. Bradley, M. Lawes, M.E. Morsy, Measurement of turbulence characteristics in a large scale fan-stirred spherical vessel, *Journal of Turbulence* 20 (2019) 195-213, doi.org/10.1080/14685248.14682019.11610566.

- [44] D. Bradley, M. Lawes, K. Liu, M.S. Mansour, Measurements and correlations of turbulent burning velocities over wide ranges of fuels and elevated pressures, *Proc. Combust. Inst.* 34 (2013) 1519-1526.
- [45] A. Bagdanavicius, P.J. Bowen, D. Bradley, M. Lawes, M.S. Mansour, Stretch rate effects and flame surface densities in premixed turbulent combustion up to 1.25 MPa, *Combust. Flame* 162 (2015) 4158-4166.
- [46] J. Göttgens, F. Mauss, N. Peters, Analytic approximations of burning velocities and flame thicknesses of lean hydrogen, methane, ethylene, ethane, acetylene, and propane flames, *Symp. (Int.) Combust.* 24 (1992) 129-135.
- [47] C. Morley, Gaseq: a chemical equilibrium program for Windows, Ver. 0.79, (2005).
- [48] D. Bradley, M. Lawes, M. Mansour, Explosion bomb measurements of ethanol–air laminar gaseous flame characteristics at pressures up to 1.4 MPa, *Combust. Flame* 156 (2009) 1462-1470.
- [49] D. Bradley, R. Hicks, M. Lawes, C. Sheppard, R. Woolley, The measurement of laminar burning velocities and Markstein numbers for iso-octane–air and iso-octane–n-heptane–air mixtures at elevated temperatures and pressures in an explosion bomb, *Combust. Flame* 115 (1998) 126-144.
- [50] M. Lawes, M.P. Ormsby, C.G. Sheppard, R. Woolley, The turbulent burning velocity of iso-octane/air mixtures, *Combustion and Flame* 159 (2012) 1949-1959.
- [51] M. Harker, T. Hattrell, M. Lawes, C. Sheppard, N. Tripathi, R. Woolley, Measurements of the three-dimensional structure of flames at low turbulence, *Combust. Sci. Technol.* 184 (2012) 1818-1837.
- [52] B. Thorne, Development of a 3D Laser Imaging System and its Application in Studies of Turbulent Flame Structure, PhD Thesis, University of Leeds, 2017.
- [53] A. Melling, Tracer particles and seeding for particle image velocimetry, *Meas. Sci. Technol.* 8 (1997) 1406.
- [54] U. Müller, M. Bollig, N. Peters, Approximations for burning velocities and Markstein numbers for lean hydrocarbon and methanol flames, *Combust. Flame* 108 (1997) 349-356.
- [55] O. Röhl, S. Jerzembeck, J. Beeckmann, N. Peters, Numerical investigation of laminar burning velocities of high octane fuel blends containing ethanol, SAE paper, , (2009).
- [56] A. Palacios, D. Bradley, Generalised correlations of blow-off and flame quenching for sub-sonic and choked jet flames, *Combust. Flame* 185 (2017) 309-318.

- [57] D. Bradley, M. Lawes, M.E. Morsy, Measurement of Turbulence Characteristics in a Large Scale Fan-Stirred Spherical Vessel, *J Turbul.* , submitted for publication., (2019).
- [58] D. Bradley, P. Gaskell, X. Gu, The mathematical modeling of liftoff and blowoff of turbulent non-premixed methane jet flames at high strain rates, *Symp. (Int.) Combust.* 27 (1998) 1199-1206.
- [59] D. Bradley, P. Gaskell, X. Gu, A. Sedaghat, Premixed flamelet modelling: Factors influencing the turbulent heat release rate source term and the turbulent burning velocity, *Combustion and Flame* 143 (2005) 227-245.
- [60] T.M. Wabel, A.W. Skiba, J.F. Driscoll, Turbulent burning velocity measurements: Extended to extreme levels of turbulence, *Proc. Combust. Inst.* 36 (2017) 1801-1808.
- [61] J. Sidey, E. Mastorakos, R. Gordon, Simulations of autoignition and laminar premixed flames in methane/air mixtures diluted with hot products, *Combust. Sci. Technol.* 186 (2014) 453-465.
- [62] X.J. Gu, M.Z. Haq, M. Lawes, R. Woolley, Laminar burning velocity and Markstein lengths of methane–air mixtures, *Combust. Flame* 121 (2000) 41-58.
- [63] Design Reaction , CHEMKIN 10131, *React. Des.*, (2013).